

Article

Quantum Spatial Search with Electric Potential: Long-Time Dynamics and Robustness to Noise

Thibault Fredon ^{1,*}, Julien Zylberman ², Pablo Arnault ¹ and Fabrice Debbasch ^{2,*}

¹ Université Paris-Saclay, CNRS, ENS Paris-Saclay, INRIA, Laboratoire Méthodes Formelles, 91190 Gif-sur-Yvette, France

² Sorbonne Université, Observatoire de Paris, Université PSL, CNRS, LERMA, 75005 Paris, France

* Correspondence: fredonthibault@gmail.com (T.F.); fabrice.debbasch@gmail.com (F.D.)

Abstract: We present various results on the scheme introduced in a previous work, which is a quantum spatial-search algorithm on a two-dimensional (2D) square spatial grid, realized with a 2D Dirac discrete-time quantum walk (DQW) coupled to a Coulomb electric field centered on the node to be found. In such a walk, the electric term acts as the oracle of the algorithm, and the free walk (i.e., without electric term) acts as the “diffusion” part, as it is called in Grover’s algorithm. The results are the following. First, we run long time simulations of this electric Dirac DQW, and observe that there is a second localization peak around the node marked by the oracle, reached in a time $O(\sqrt{N})$, where N is the number of nodes of the 2D grid, with a localization probability scaling as $O(1/\ln N)$. This matches the state-of-the-art 2D-DQW search algorithms before amplitude amplification. We then study the effect of adding noise on the Coulomb potential, and observe that the walk, especially the second localization peak, is highly robust to spatial noise, more modestly robust to spatiotemporal noise, and that the first localization peak is even highly robust to spatiotemporal noise.

Keywords: quantum algorithms; quantum walks; quantum spatial search; noise



Citation: Fredon, T.; Zylberman, J.; Arnault, P.; Debbasch, F. Quantum Spatial Search with Electric Potential: Long-Time Dynamics and Robustness to Noise. *Entropy* **2022**, *24*, 1778. <https://doi.org/10.3390/e24121778>

Academic Editors: Giuliano Benenti and Brian R. La Cour

Received: 24 October 2022

Accepted: 30 November 2022

Published: 5 December 2022

Publisher’s Note: MDPI stays neutral with regard to jurisdictional claims in published maps and institutional affiliations.



Copyright: © 2022 by the authors. Licensee MDPI, Basel, Switzerland. This article is an open access article distributed under the terms and conditions of the Creative Commons Attribution (CC BY) license (<https://creativecommons.org/licenses/by/4.0/>).

1. Introduction

Discrete-time quantum walks (DQWs) correspond to the one-particle sector of quantum cellular automata [1,2]. They can simulate numerous physical systems, ranging from particles in arbitrary Yang–Mills gauge fields [3] and massless Dirac fermions near black holes [4], to charged quantum fluids [5], see also Refs. [6–16] for other physics-oriented applications.

Moreover, DQWs can be seen as quantum analogs of classical random walks (CRWs) [17], and can be used to build spatial-search algorithms that outperform [18] those built with CRWs. Continuous-time quantum walks can also be used for such a purpose [19]. In three spatial dimensions, DQW-based algorithms [18,19] find the location of a marked node with a constant localization probability (We call “localization probability” the probability to be at the marked node, or nodes if there are several of them.) after $O(\sqrt{N})$ time steps, with N , the number of nodes of the three-dimensional grid, and this is exactly the bound reached by Grover’s algorithm [20–25]. However, no two-dimensional (2D) QW proposed so far reaches Grover’s lower bound.

The state-of-the-art result using a 2D DQW was obtained by Tulsi in Ref. [26]: Tulsi’s algorithm finds a marked node with a localization probability scaling as $O(1/\ln N)$ in $O(\sqrt{N})$ time steps, where N is the total number of nodes. To reach a probability independent of N , several amplitude amplification time steps have to be performed after the quantum-walk part. These extra time steps are Grover’s algorithm time steps, see Ref. [27]. Taking the amplitude amplification into account, Tulsi’s algorithm reaches an $O(1)$ localization probability after $O(\sqrt{N \ln N})$ time steps.

Other schemes of 2D DQW for spatial search have followed, such as the one by Roget et al. in Ref. [28], where the 2D DQW simulates a massless Dirac fermion on a grid

with defects. This scheme is inspired by physics, and it reaches Tulsi's bound using a coin of dimension 2 instead of 4. Recently, Zylberman and Debbasch introduced in Ref. [29] a new DQW scheme for 2D quantum spatial search. This scheme implements quantum search by simulating the dynamics of a massless Dirac fermion in a Coulomb electric field centered on the nodes to be found. We call this DQW "electric Dirac DQW" (We call "Dirac DQW" a DQW that has as a continuum limit the Dirac equation. Throughout this paper, the terminology "electric Dirac DQW" will always refer to a Dirac DQW coupled to a Coulomb electric potential, unless otherwise stated. In the literature, other types of electric potentials have been considered. The reason why we do not specify the term "Coulomb" in the present denomination "electric Dirac DQW" is because the idea we want to convey is that the marked node is encoded in the shape of the electric potential, but the precise form of the electric potential, e.g., here, the fact that it is a Coulomb potential, may not be that relevant.). In this walk, the oracle is a position-dependent *phase*.

This oracle is diagonal in the position basis and can be efficiently implemented on n qubits up to an error ϵ using $O(\frac{1}{\epsilon})$ primitive quantum gates [30]. This total number of quantum gates is independent of n and makes possible the implementation of the oracle on current Noisy Intermediate Scale Quantum (NISQ) devices and on future universal quantum computers.

Note also that the algorithm proposed in Ref. [29] actually constitutes a paradigm change in the construction of search algorithms, because it is based on the physically motivated idea that the position of the marked node can be encoded in the shape of an artificial force field, which acts on the quantum walker.

One of the main results of Zylberman and Debbasch's paper [29] is a localization probability, which displays a maximum in $O_{N \rightarrow \infty}(1)$ time steps, the localization probability scaling as $O(1/N)$ (a detailed analysis is presented in Section 3). Since it focuses on this result, Ref. [29] does not offer an analysis of the walk at times much larger than $O(1)$. Moreover, practical implementation not only on current NISQ devices, but also on future, circuit-based quantum computers, can only be envisaged if the algorithm is robust to noise (see, for example, Refs. [5,31–37]); this question is also not addressed in Ref. [29].

The aim of this article is to explore both aspects: long-time dynamics and robustness to noise. The main results are the following. First, the electric Dirac DQW exhibits a second localization peak at a time scaling as $O(\sqrt{N})$ with localization probability scaling as $O(1/\ln N)$. This makes this walk state-of-the-art for 2D DQW spatial search before amplitude amplification. Moreover, this second localization peak is highly robust to spatial noise. Finally, the peak is also robust to spatiotemporal noise, but not as much as it is to time-independent spatial noise.

The article is organized as follows. In Section 2, we offer a review of the electric Dirac DQW presented in Ref. [29]. In Section 3, we study in detail the first two maxima of the localization probability. We show that the first maximum, already analyzed in Ref. [29], is actually present up to $N = 9 \times 10^6 > 10^6 \simeq 2^{20}$ (have in mind that 20 is the current average number of working qubits on most IBM-Q platforms according to <https://quantum-computing.ibm.com/services/resources> accessed on 29 November 2022). We also present evidence for the scaling laws characterizing both the first peak and the second, long-time peak, which reaches Tulsi's state-of-the-art bound. In Section 4, we analyze the resources one needs to implement the quantum spatial search in terms of qubits and primitive quantum operations. In Section 5, we show that the walk, and in particular the second peak, have a good robustness to spatial oracle noise. We also show that the first peak is robust even to spatiotemporal noise. In Section 6, we propose an analysis of the walker's probability distributions. These probability distributions show that the spatial noise does not affect the shape of the peaks significantly. The peaks remain extremely high relative to the background, which shows not only good but high robustness of the peaks to spatial oracle noise. The probability distributions also show that the second peak is sharper than the first one.

2. Basics

2.1. Definition of the 2D Electric Dirac DQW

We consider a 2D square spatial grid with nodes indexed by two integers $(p, q) \in \llbracket 0, M \rrbracket^2$, where $M \in \mathbb{N}$ is the number of nodes along one dimension and $N = M^2$ is the total number of nodes. The time is also discrete and indexed by a label $j \in \mathbb{N}$. The walker is defined by its quantum state $|\Psi_j\rangle$ in the Hilbert space $\mathcal{H}_C \otimes \mathcal{H}_p$, where \mathcal{H}_C , called *coin space*, is the two-dimensional Hilbert space, which corresponds to the internal, coin degree of freedom, and \mathcal{H}_p , called *position space*, corresponds to the spatial degrees of freedom. The *wavefunction* of the state will be denoted as $\Psi_{j,p,q} \equiv (\psi_{j,p,q}^L \quad \psi_{j,p,q}^R)^\top$, where \top denotes the transposition. The discrete-time evolution of the walker is defined by the following one-step evolution equation,

$$\Psi_{j+1,p,q} = (\mathcal{U}\Psi_j)_{p,q}. \tag{1}$$

The one-step evolution operator, also called *walk operator*, \mathcal{U} , is defined by

$$\mathcal{U} := e^{-ie\phi} R(\theta^-) \mathcal{S}_2 R(\theta^+) \mathcal{S}_1, \tag{2}$$

where $\mathcal{S}_{1,2}$ are standard *shift operators*,

$$(\mathcal{S}_1 \Psi)_{p,q}^L := \psi_{p+1,q}^L \tag{3a}$$

$$(\mathcal{S}_1 \Psi)_{p,q}^R := \psi_{p-1,q}^R \tag{3b}$$

$$(\mathcal{S}_2 \Psi)_{p,q}^L := \psi_{p,q+1}^L \tag{3c}$$

$$(\mathcal{S}_2 \Psi)_{p,q}^R := \psi_{p,q-1}^R, \tag{3d}$$

$R(\theta)$ is a coin-space rotation, also called *coin operator*, defined by

$$R(\theta) := \begin{bmatrix} \cos \theta & i \sin \theta \\ i \sin \theta & \cos \theta \end{bmatrix}, \tag{4}$$

and

$$\theta^\pm := \pm \frac{\pi}{4} - \frac{\mu}{2}, \tag{5}$$

with μ , some real parameter. A schematic representation of a quantum circuit for \mathcal{U} is proposed in Figure 1. More details about the circuit are given in Section 4. A schematized picture of the walk operator is proposed in Figure 2.

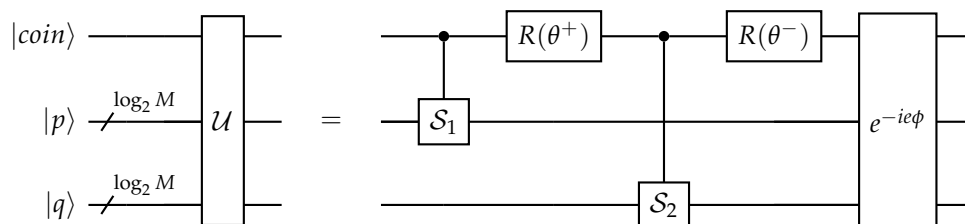


Figure 1. Quantum circuit of a single step operator \mathcal{U} .

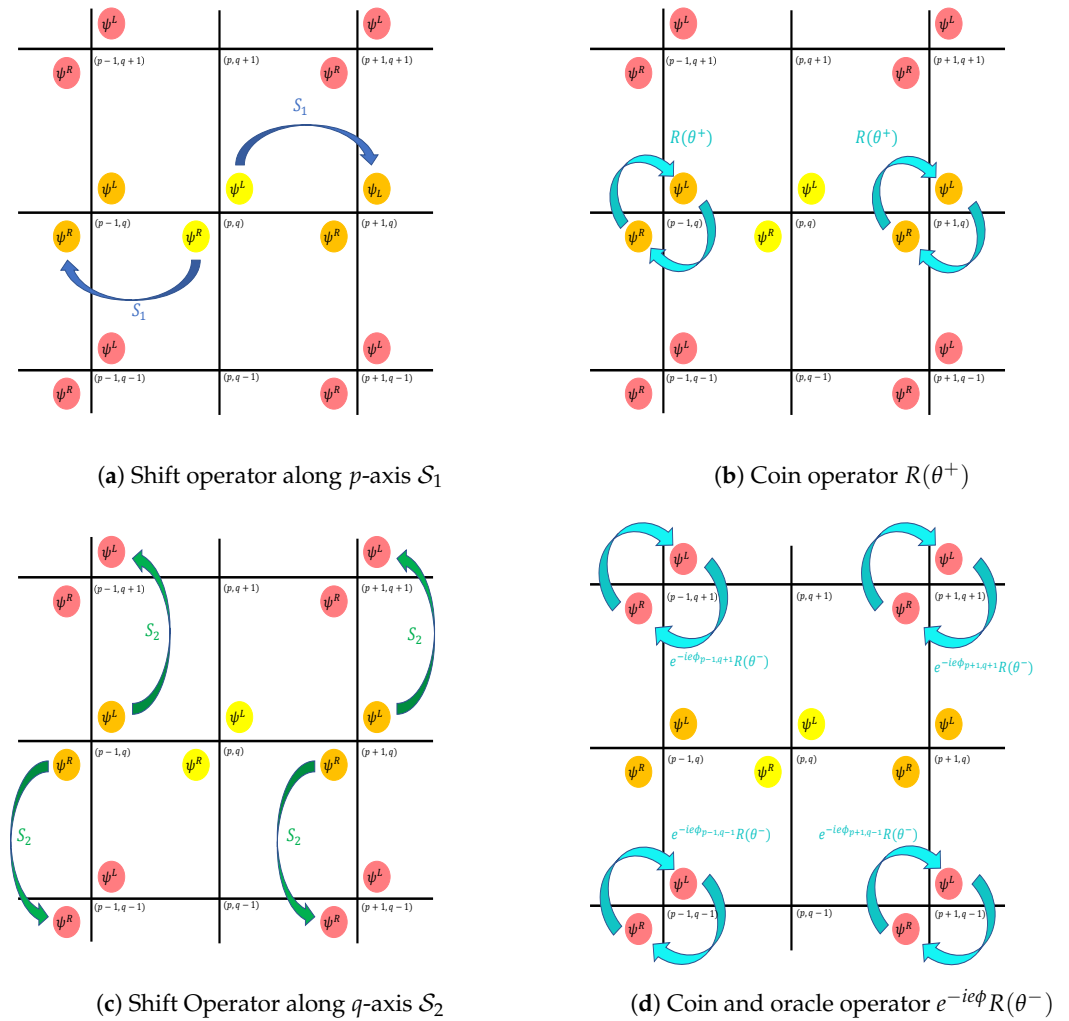


Figure 2. Schematic representation of the quantum walk scheme for one step, starting from position (p, q) . **(a)** First, the S_1 shift operator is applied, shifting the ψ^L component at position (p, q) to position $(p + 1, q)$ and the ψ^R component at position (p, q) to position $(p - 1, q)$. **(b)** Second, the rotation $R(\theta^+)$ is applied at positions $(p \pm 1, q)$, mixing the two components ψ^L and ψ^R (see Equation (4) with angle θ^+). **(c)** Third, the S_2 shift operator is applied, shifting the ψ^L components at positions $(p \pm 1, q)$ to positions $(p \pm 1, q + 1)$ and the ψ^R components at position $(p \pm 1, q)$ to position $(p \pm 1, q - 1)$. **(d)** Finally, the rotation $R(\theta^-)$ and the oracle $e^{-ie\phi}$ is applied. The two components ψ^L and ψ^R are first mixed by the rotation defined Equation (4) with angle θ^- and then multiplied by the position-dependent phase factor defined by the potential ϕ . In this scheme, these operations are illustrated by considering the components $\psi_{p,q}^L$ and $\psi_{p,q}^R$ at a node (p, q) . At the end of one step, the components $\psi_{p,q}^L$ and $\psi_{p,q}^R$ are spread at the nodes $(p + 1, q + 1)$, $(p + 1, q - 1)$, $(p - 1, q + 1)$, and $(p - 1, q - 1)$ in a unitary manner.

The operator $e^{-ie\phi}$ is diagonal in position space, i.e., it acts on Ψ_j as

$$(e^{-ie\phi}\Psi_j)_{p,q} = e^{-ie\phi_{p,q}}\Psi_{j,p,q}, \tag{6}$$

with $\phi : (p, q) \mapsto \phi_{p,q} \in \mathbb{R}$ some sequence of the lattice position, and e , a parameter that we can call the charge of the walker, see why further down. The sequence ϕ can be called the lattice electric potential for at least two reasons: (i) in the continuum limit (see below, Section 2.2), this sequence indeed becomes, mathematically, an electric potential coupled to the walker, who then obeys the Dirac equation, and (ii) beyond the continuum limit, it has been shown that similar 2D DQWs exhibit an exact lattice U(1) gauge invariance [38]

which, in the continuum limit, becomes the standard U(1) gauge invariance of the Dirac equation coupled to an electromagnetic potential.

2.2. Continuum Limit

We introduce a spacetime-lattice spacing ϵ , and coordinates $t_j := \epsilon j$, $x_p := \epsilon p$, and $y_q := \epsilon q$ [39,40]. We assume that $\Psi_{j,p,q}$ coincides with the value taken at point t_j , x_p , and y_q by a function Ψ of the continuous coordinates t , x , and y . We are interested in the dynamics followed by Ψ when $\epsilon \rightarrow 0$. Let us introduce the following continuum quantities,

$$m := \frac{\mu}{\epsilon} \tag{7a}$$

$$V(x_p, y_q) := \frac{\phi_{p,q}}{\epsilon}, \tag{7b}$$

which are, respectively, the mass and electric potential, see why just below.

Expand now Equation (1) in ϵ around $\epsilon = 0$. The walk operator, Equation (2), has been chosen so that (i) the zeroth-order terms give us $\Psi(t, x, y) = \Psi(t, x, y)$, i.e., the terms cancel each other, and (ii) the first-order terms deliver the well-known Dirac equation coupled to an electric potential V . This equation (in natural units where $c = 1$ and $\hbar = 1$) reads:

$$i\partial_t \Psi = \mathcal{H} \Psi, \tag{8}$$

where the Dirac Hamiltonian is

$$\mathcal{H} := \alpha^k (-i\partial_k) + m\alpha^0 + eV, \tag{9}$$

where summation over $k = 1, 2$ is implicitly assumed. The alpha matrices are

$$\alpha^0 := \sigma_x \tag{10a}$$

$$\alpha^1 := \sigma_z \tag{10b}$$

$$\alpha^2 := -\sigma_y, \tag{10c}$$

where the σ s are the Pauli matrices. Thus, this DQW, Equation (1), simulates the (1+2)D Dirac equation coupled to an electric potential, explaining why the ‘‘Dirac DQW’’ is called an electric DQW.

2.3. Coulomb Potential

As shown in Equation (8), the sequence $\phi = \epsilon V$ represents in the continuum limit the electric potential to which the walker is coupled. We choose V to be a Coulomb potential created by a point particle of charge Q at location (Ω_x, Ω_y) on the 2D plane:

$$eV(x, y) := \frac{eQ}{\sqrt{(x - \Omega_x)^2 + (y - \Omega_y)^2}}. \tag{11}$$

For the sake of simplicity, e will be set to -1 . As discussed in Ref. [29], one can take, without loss of generality (i) $(\Omega_x, \Omega_y) = (\frac{M}{2} - \frac{1}{2}, \frac{M}{2} - \frac{1}{2})$, which is called the *center*, and (ii) $\epsilon = 1$. The charge Q is set to 0.9, and $m = \mu = 0$. Notice that the center is not located on a node of the 2D lattice; it is at equal distance of the four nodes, namely, $(\frac{M}{2}, \frac{M}{2})$, $(\frac{M}{2} - 1, \frac{M}{2})$, $(\frac{M}{2}, \frac{M}{2} - 1)$, and $(\frac{M}{2} - 1, \frac{M}{2} - 1)$. With this choice of potential, the walk can be referred to as a ‘‘Coulomb walk’’.

2.4. Definition of the Spatial-Search Problem

The spatial-search problem is defined as follows. Consider at time $j = 0$ a fully delocalized walker on the grid, i.e., $\forall (p, q, a) \in \llbracket 0, M \rrbracket^2 \times \{L, R\}$, $\psi_{0,p,q}^a := \frac{1}{M\sqrt{2}}$. The

problem addressed by the Coulomb walk with this initial condition is: can the walker localize on the nodes where $\phi_{p,q}$ is at its extremum, that is, the four nodes around the center $(\Omega_x, \Omega_y) = (\frac{M}{2} - \frac{1}{2}, \frac{M}{2} - \frac{1}{2})$?

The first observable will be the probability of being on these nodes as a function of time and of the number of grid nodes:

$$P_j(N) := \sum_{(p',q') \in \{\pm\frac{1}{2}\}^2} \left\| \Psi_{j, \Omega_x+p', \Omega_y+q'}(N) \right\|^2, \tag{12}$$

which we call *localization probability*. It has been shown in Ref. [29] that the localization probability admits a first maximum at time $j_1(N) = 82$, independent of N . We now define long times as times t_j with j much larger than 82. The long-time behavior is studied below in Section 3.

We consider the *probability distribution* over space as second observable,

$$d_{j,p,q}(N) := \left\| \Psi_{j,p,q}(N) \right\|^2, \tag{13}$$

which is studied in Section 6.

The fully delocalized initial condition is common in spatial-search problems because of Grover’s algorithm [20]. Moreover, this initial condition can easily be implemented on a quantum circuit as a tower of Hadamard gates. Other initial superpositions for the coin part were considered in Ref. [29]. Now, the fully delocalized initial condition forces us to pay attention to boundary conditions. In our work, we choose periodic boundary conditions. From a computer science point of view, one can expect from a database to have a list of addresses, which are on a graph whose ends are connected, corresponding exactly to periodic boundary conditions.

3. Noiseless Case: Long Times

In Ref. [29], it is shown that for a ‘small’ grid (up to $N = 2.5 \times 10^5$), the first maximum occurs at $j_1(N) = 82 = O_{N \rightarrow \infty}(1)$ with a localization probability $P_{j_1(N)}(N)$ scaling as $O(1/N)$. According to Figure 3, the result $j_1(N) = O(1)$ actually holds up to $N = 9 \times 10^6 \simeq 10^7$. The left panel of Figure 4 shows that $P_{j_1(N)}(N) = O(1/N)$ is valid up to $N = 900 \times 900 \simeq 10^6$. Now, $P_j(N)$ with fixed N presents several other maxima as j varies, and Figure 4 shows in particular that there is a prominent second maximum. This second maximum occurs at a time $j_2(N)$ which, according to Figure 3 and to the right panel of Figure 4 scales as $O(\sqrt{N})$. The right panel of Figure 4 also shows the localization probability $P_{j_2(N)}(N) = O(1/\ln N)$. This result matches the state-of-the-art result in 2D DQW search algorithms before amplitude amplification [26].

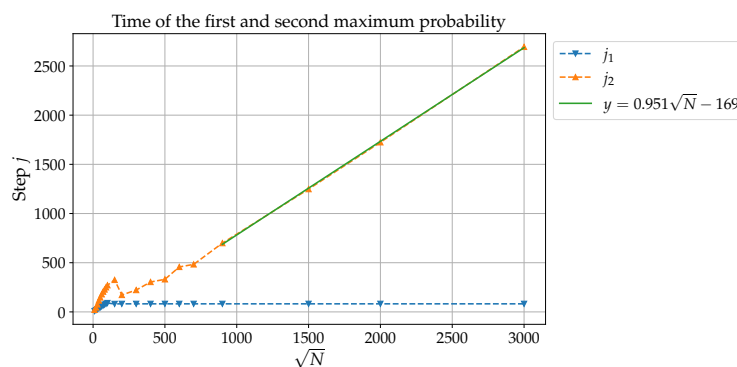


Figure 3. Times j_1 (blue) and j_2 (orange) at which the localization probability $P_j(N)$ reaches a maximum, plotted as a function of \sqrt{N} for $m = 0, e = -1$, and $Q = 0.9$.

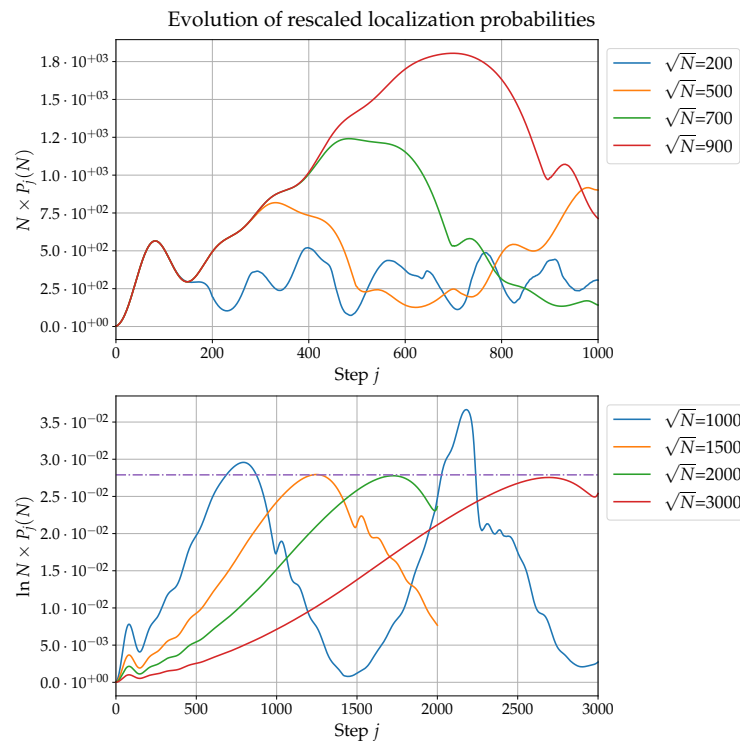


Figure 4. Rescaled localization probability $P_j(N)$ for $m = 0$, $e = -1$, and $Q = 0.9$. Left panel: $P_j(N) \times N$ as a function of j , for several values of N . Right panel: $P_j(N) \times \ln N$ as a function of j , for different values of N .

4. Resource Analysis

Since the evolution operator of the Coulomb walk is built out of two 1D shift operators, one for each spatial directions, the Coulomb walk only requires a 2-dimensional coin space. On the contrary, Tulsi’s walk (see Ref. [26]) uses a 2D shift operator, which requires a 4-dimensional Hilbert space for the coin, so encoding this walk requires one more qubit than encoding the walk studied in the present article. Also note that Tulsi’s algorithm also uses an ancilla qubit to allow a part of the probability amplitude to remain on the same site after one evolution step (technically, Tulsi’s walk uses a controlled shift operator and a controlled coin operator with respect to the ancilla). Thus, in total, Tulsi’s algorithm needs two more qubits than the Coulomb walk to perform a quantum spatial search on a database of the same size. Roget et al.’s walk, presented in Ref. [28], is a DQW—as is the Coulomb walk. It also uses two 1D shift operators and dispenses with the ancilla qubit. The difference with the Coulomb walk lies in the choice of oracle. The Coulomb walk uses an artificial electric field as oracle, while Roget et al.’s walk views the node to be found as a defect and therefore replaces on the defect the rotation $R(\theta)$ of Equation (4) by the identity operator.

A scheme implementing efficiently (up to a given precision ϵ) position-dependent diagonal unitaries similar to the electric potential oracle in Equation (6) can be found in J. Welsh et al. (Ref. [30]). The total number n of one-qubit and two-qubit quantum operations used in this scheme scales as $O(\frac{1}{\epsilon})$ and is actually independent of n . However, the implementation of the shift operators $S_{1,2}$ (see Equation (3)) requires a number of primitive quantum operations, which does depend on n and scales as $O(n^2)$ because implementing shift operators requires performing Quantum Fourier Transforms (QFTs) [41]. Note that each coin operation $R(\theta^-)$ and $R(\theta^+)$ in Equation (2) can be implemented as only one single quantum gate on the coin qubit.

5. Oracle Noise

Today, one of the main goals in quantum computing is having fault-tolerant algorithms, which can be implemented on NISQ devices [42–44].

In the scheme developed by Welch et al. in Ref. [30], the final quantum circuit of the oracle is composed of *CNOT* and R_Z . The rotation angles are only implementable up to a finite accuracy due to hardware limitations. This generates fluctuations in the potential ϕ and we model these fluctuations by a white noise. More precisely, we replace $\phi_{p,q}$ by $\phi_{j,p,q}^B = \phi_{p,q} + B_{j,p,q}$, where B is a white noise in all its variables. To make things as simple as possible, given a point (j, p, q) , $B_{j,p,q}$ is chosen randomly with uniform distribution in a certain interval $(-B_{\max}, B_{\max})$ independent of (j, p, q) . Noise that depends on time only does not modify the probability distribution. All noises considered in this article will therefore be space-dependent. We will first focus on time-independent, but space-dependent noise, and then switch to both time- and space-dependent noise.

Note that decoherence noise on the free-walk part and on Grover search has already been studied in Refs. [45–51].

The amplitude of the noise is best characterized by the noise-to-signal ratio:

$$r := \frac{B_{\max}}{\max_{p,q} |\phi_{p,q}|} . \tag{14}$$

5.1. Spatial Oracle Noise

In this subsection, all observables are averaged over 50 realizations of the noise. Figure 5 presents results obtained for $N = 200^2$ and $N = 500^2$. When the noise-to-signal ratio r is not too high, say $r \lesssim 0.5$, both peaks still exist and the second one occurs slightly later, with approximately the same time delay with respect to the noiseless situation. The amplitude of the peaks is also affected by the noise. In particular, for large enough N (see the right panel in Figure 5), the amplitude of the first peak decreases while the amplitude of the second peak actually increases. Thus, weak noise favors, and even enhances the second peak, at least for large enough values of N . Increasing the noise-to-signal ratio r erases the first peak and, to a certain extent, also the second one. Note however that, for large enough N , the probability $P_j^r(N)$ still exhibits a (rather flat) maximum in lieu of the second peak. So, in any case, noise favors the second peak. So, all in all, the algorithm studied in this article shows good to great robustness to spatial noise. It is also instructive to investigate this robustness through the probability distribution over space $d_{j,p,q}^r(N)$ and this is done in Section 6 below.

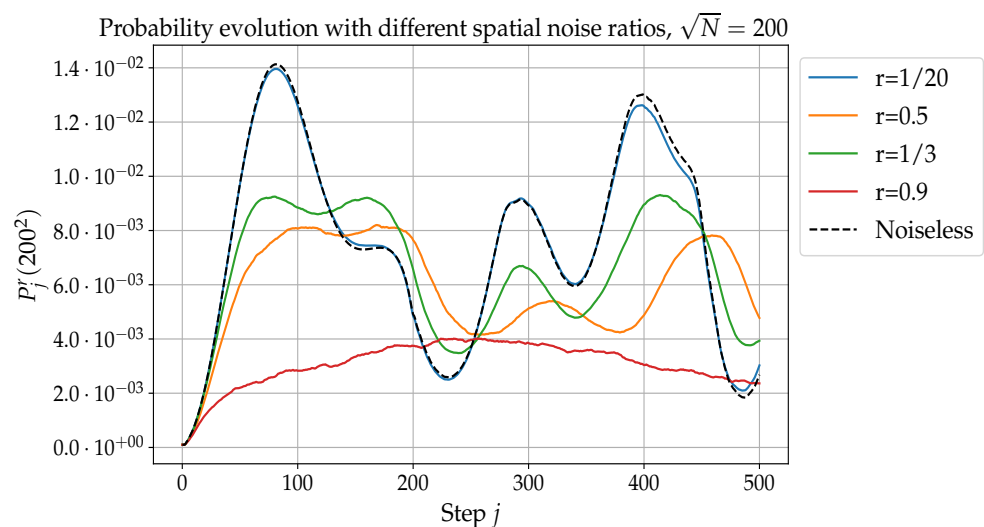


Figure 5. Cont.

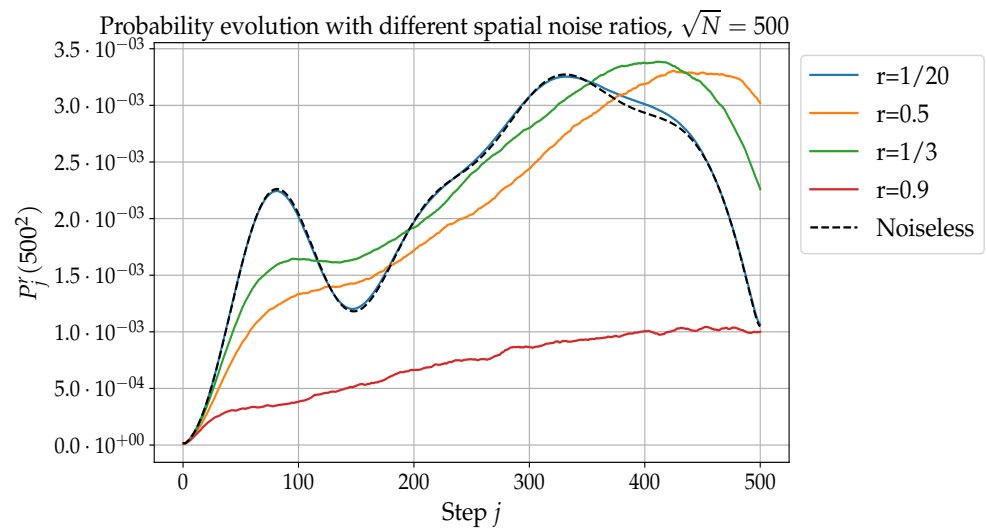


Figure 5. Localization probability $P_j^r(N)$ with spatial noise as a function of j , for different noise-to-signal ratios r , for $m = 0, e = -1, Q = 0.9$, and $\sqrt{N} = 200$ (top) and $\sqrt{N} = 500$ (bottom).

5.2. Spatiotemporal Oracle Noise

In this subsection, all observables are averaged over 10 realizations of the noise. Numerical results are presented in Figure 6. One first observes a global decreases in the localization probability, which gets globally lower with increasing r . However, it also appears that the first peak is less impacted by the noise than the rest of the curve, and especially the second peak. This can be understood in the following way. Since the noise we are considering is white in both space and time, the central limit theorem applies. The walk will therefore exhibit diffusive behavior in the ‘long’-time limit (see, for example, Ref. [49]).

However, the shorter the time, the less important the perturbation induced by the noise on the walk’s behavior. The striking robustness of the first peak, which always occur at $j = 82$, indicates that $j = 82$ is a ‘short’ time, at least for noise-to-signal ratios exceeding 0.5.

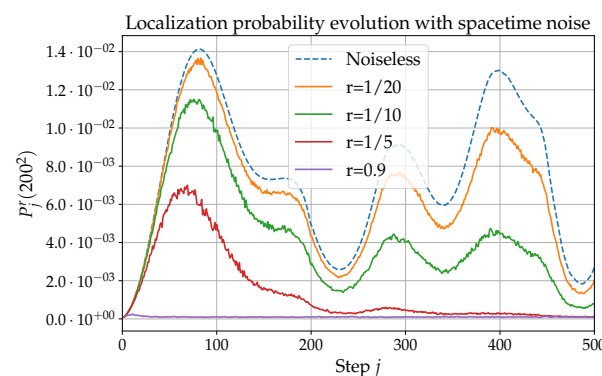


Figure 6. Localization probability $P_j^r(200^2)$ as a function of j for different spatiotemporal noise-to-signal ratios r , with $m = 0, e = -1$, and $Q = 0.9$.

6. Probability Distribution in Space

We now investigate the probability distribution $D_j = \{d_{j,p,q}, \{p, q\} \in \llbracket 0; M \rrbracket^2\}$ of the walk at the localization times j_1 and j_2 corresponding to the first and second peak. The height ratio η between the peak and the background is defined as

$$\eta_j(N) := \frac{d_{j, \frac{M}{2}-1, \frac{M}{2}-1}(N)}{d_{j,1,1}(N)}, \tag{15}$$

where $d_{j, \frac{M}{2}-1, \frac{M}{2}-1}(N)$ is the probability to be on one of the four nodes of interest (where the potential is maximum), and where $d_{j,1,1}(N)$ is the probability to be where the potential is the weakest.

6.1. Noiseless Case

The noiseless case is presented in Figure 7. The probability distributions are sharply peaked on the nodes of interest for both $j = j_1$ (top plots) and $j = j_2$ (bottom plots). For a small grid size (i.e., $\sqrt{N} = 200$), the height ratio is better for the first peak than for the second peak (the precise values are given in the figure caption). For a larger grid size (i.e., $\sqrt{N} = 500$ and $\sqrt{N} = 1000$), the height ratio of the first peak is important, but that of the second peak is substantially larger (see the figure caption).

6.2. Spatial Oracle Noise

Let us now investigate the probability density $D_j^r = \{d_{j,p,q}^r, \{p,q\} \in \llbracket 0, M \rrbracket\}$ in the presence of noise with noise-to-signal ratio r . Figure 8 displays D_j^r (top plots) and $D_j^r - D_j$ (bottom plots) at $j = j_1$ (left plots) and $j = j_2$ (right plots). On the top plots of Figure 8, where $D_j^{1/3}$ for $r = 1/3$ is plotted, one observes that the overall shapes of the peaks, and in particular their widths, are not affected by the noise. The height ratios (given in the caption of Figure 8) are still very large, even in the presence of a substantial amount of noise ($r = 1/3$). This shows *not only good, but high robustness* of the walk to spatial noise. Looking at the bottom plots of Figure 8 one observes that noise makes the first peak lower (two bottom left plots), but makes the second peak (two bottom right plots) higher for a small grid size ($M = 200$) or balanced between the four nodes of interest for a larger grid size ($M = 500$). These observations are of course consistent with the curves of Figure 5.

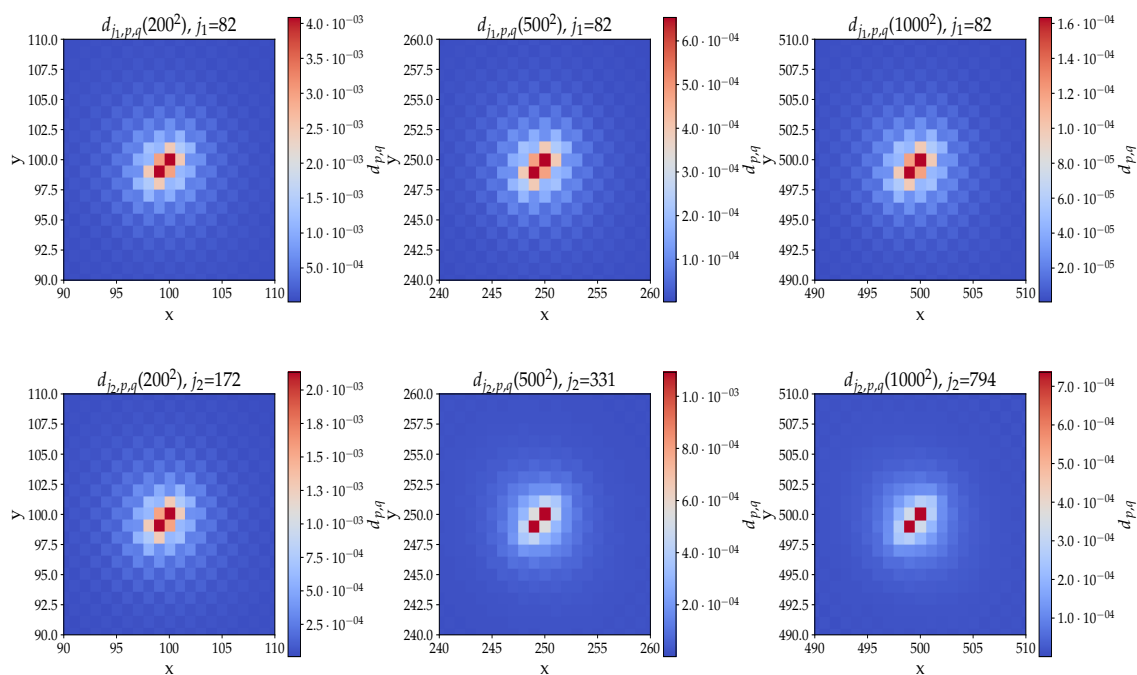


Figure 7. Probability distribution D_j in the noiseless case for $\sqrt{N} = 200, 500, 1000$, $j = j_1$ (top plots), and $j = j_2$ (bottom plots) and $m = 0, e = -1, Q = 0.9$. Height ratios for j_1 : $\eta_{j_1}(200^2) = 160$, $\eta_{j_1}(500^2) = 163$, and $\eta_{j_1}(1000^2) = 163$. Height ratios for j_2 : $\eta_{j_2}(200^2) = 127$, $\eta_{j_2}(500^2) = 242$, and $\eta_{j_2}(1000^2) = 1933$.

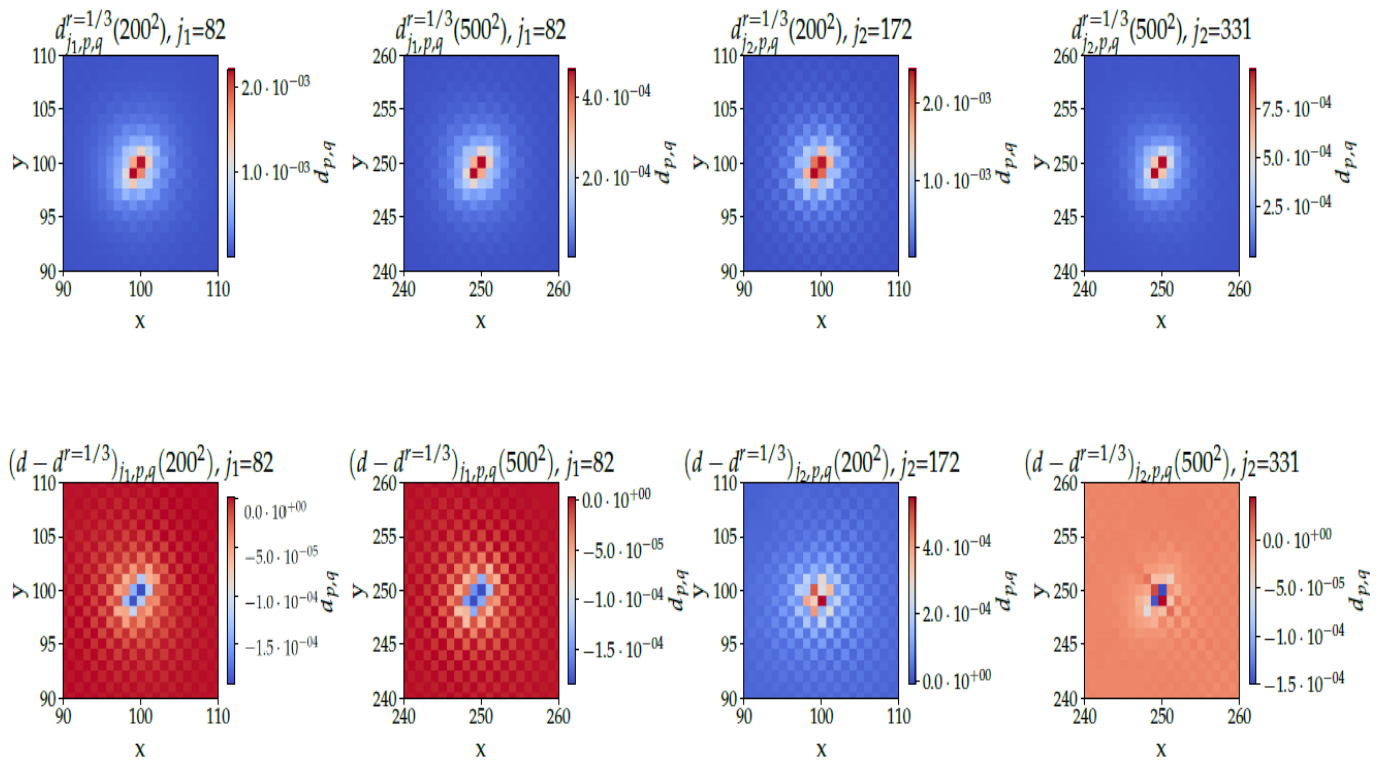


Figure 8. **Top** plots: Probability distribution $d_{j,p,q}^{r=1/3}(N)$ for $\sqrt{N} = 200$ and 500 , at j_1 (left plots) and j_2 (right plots), averaged over 50 realizations of the spatial noise, with $m = 0, e = -1, Q = 0.9$. Height ratios for j_1 : $\eta_{j_1}^{r=1/3}(200^2) = 87$ and $\eta_{j_1}^{r=1/3}(500^2) = 115$. Height ratios for j_2 : $\eta_{j_2}^{r=1/3}(200^2) = 142$ and $\eta_{j_2}^{r=1/3}(500^2) = 218$. **Bottom** plots: Difference $d_{j,p,q}^{r=1/3}(N) - d_{j,p,q}(N)$ between the noisy and the noiseless cases, for $m = 0, e = -1, Q = 0.9$.

7. Conclusions and Discussion

In this paper, we have shown that the 2D electric Dirac DQW presented in Ref. [29] has at least two different localization peaks: (i) one at short times ($O_{N \rightarrow \infty}(1)$ with N the number of nodes on the 2D grid), for which the localization probability scales as $O(1/N)$, and (ii) another at a time scaling as $O(\sqrt{N})$ with localization probability in $O(1/\ln N)$, which matches the state-of-the-art result in spatial search with 2D DQWs before amplitude amplification [26,28]. This dynamic was studied numerically up to $N = 9 \times 10^6 \simeq 2^{20}$.

This quantum spatial search also presents a memory advantage by formally requiring two qubits less than Tulsı’s algorithm. In terms of quantum operations, the oracle can be efficiently implemented on a quantum circuit up to an error ϵ using $O(\frac{1}{\epsilon})$ primitive quantum gates, allowing its implementation on current NISQ devices and future fault-tolerant universal quantum computers.

We have also explored the effect of oracle noise by adding a white noise to the electric potential. This white noise can be viewed, for example, as a model of the fluctuations induced by the finite accuracy implementation of the quantum rotations involved in the Oracle quantum circuit [30]. Our results demonstrate that the algorithm is highly robust to oracle noise. The second peak is not only highly robust to, but actually slightly amplified by, spatial noise. The second peak is admittedly less robust to spatiotemporal noise but the first peak turns out highly robust to this type of noise. This study is thus very encouraging for the future implementation of quantum spatial search with electric potential on universal quantum computers and NISQ devices.

Adapting to the present walk, the ancilla technique used in Tulsı’s walk may make the second peak appear sooner and might eventually help the walk reach Grover’s lower bound. Furthermore, studying the evolution of the localization probability under other kinds of noises is assuredly very promising to extend the robustness properties of the

quantum spatial search with electric potential. Finally, extending all results to higher dimensions and to walks using other fields such as oracle will certainly prove interesting.

Author Contributions: Conceptualization, T.F., J.Z., P.A. and F.D.; Methodology, T.F., J.Z., P.A. and F.D.; Software, T.F.; Validation, P.A. and F.D.; Formal analysis, T.F., J.Z., P.A. and F.D.; Investigation, T.F., J.Z., P.A. and F.D.; Resources, T.F., P.A. and F.D.; Data curation, T.F.; Writing—original draft, T.F., J.Z., P.A. and F.D.; Writing—review & editing, T.F., J.Z., P.A. and F.D.; Visualization, F.D.; Supervision, P.A. and F.D.; Project administration, P.A. and F.D.; Funding acquisition, P.A. and F.D. All authors have read and agreed to the published version of the manuscript.

Funding: This research received no external funding.

Data Availability Statement: Data are available on reasonable demand at fredonthibault@gmail.com.

Conflicts of Interest: The authors declare no conflict of interest. The funders had no role in the design of the study; in the collection, analyses, or interpretation of data; in the writing of the manuscript; or in the decision to publish the results.

Abbreviations

The following abbreviations are used in this manuscript:

DQW	Discrete-Time Quantum Walk
QW	Quantum Walk
CQW	Continuous-Time Quantum Walk
NISQ	Noisy Intermediate Scale Quantum

References

1. Arrighi, P. An overview of quantum cellular automata. *Nat. Comput.* **2019**, *18*, 885–899. [[CrossRef](#)]
2. Farrelly, T. A review of Quantum Cellular Automata. *Quantum* **2020**, *4*, 368. [[CrossRef](#)]
3. Arnault, P.; Di Molfetta, G.; Brachet, M.; Debbasch, F. Quantum walks and non-Abelian discrete gauge theory. *Phys. Rev. A* **2016**, *94*, 012335. [[CrossRef](#)]
4. Di Molfetta, G.; Brachet, M.; Debbasch, F. Quantum walks as massless Dirac fermions in curved space-time. *Phys. Rev. A* **2013**, *88*, 042301. [[CrossRef](#)]
5. Zylberman, J.; Di Molfetta, G.; Brachet, M.; Loureiro, N.F.; Debbasch, F. Quantum simulations of hydrodynamics via the Madelung transformation. *Phys. Rev. A* **2022**, *106*, 032408. [[CrossRef](#)]
6. Berry, S.D.; Wang, J.B. Two-particle quantum walks: Entanglement and graph isomorphism testing. *Phys. Rev. A* **2011**, *83*, 042317. [[CrossRef](#)]
7. Ahlbrecht, A.; Alberti, A.; Meschede, D.; Scholz, V.B.; Werner, A.H.; Werner, R.F. Molecular binding in interacting quantum walks. *New J. Phys.* **2012**, *14*, 073050. [[CrossRef](#)]
8. Shikano, Y.; Wada, T.; Horikawa, J. Discrete-time quantum walk with feed-forward quantum coin. *Sci. Rep.-UK* **2014**, *4*, 4427. [[CrossRef](#)]
9. Bisio, A.; D’Ariano, G.M.; Perinotti, P.; Tosini, A. Weyl, Dirac and Maxwell Quantum Cellular Automata. *Found. Phys.* **2015**, *45*, 1203–1221. [[CrossRef](#)]
10. Di Molfetta, G.; Pérez, A. Quantum walks as simulators of neutrino oscillations in a vacuum and matter. *New J. Phys.* **2016**, *18*, 103038. [[CrossRef](#)]
11. Bisio, A.; D’Ariano, G.M.; Perinotti, P. Quantum cellular automaton theory of light. *Ann. Phys.-NY* **2016**, *368*, 177–190. [[CrossRef](#)]
12. Rakovszky, T.; Asbóth, J.K.; Alberti, A. Detecting topological invariants in chiral symmetric insulators via losses. *Phys. Rev. B* **2017**, *95*, 201407. [[CrossRef](#)]
13. Márquez-Martín, I.; Arnault, P.; Di Molfetta, G.; Pérez, A. Electromagnetic lattice gauge invariance in two-dimensional discrete-time quantum walks. *Phys. Rev. A* **2018**, *98*, 032333. [[CrossRef](#)]
14. Arrighi, P.; Di Molfetta, G.; Márquez-Martín, I.; Pérez, A. From curved spacetime to spacetime-dependent local unitaries over the honeycomb and triangular quantum walks. *Sci. Rep.-UK* **2019**, *9*, 10904. [[CrossRef](#)]
15. Jay, G.; Debbasch, F.; Wang, J.B. Dirac quantum walks on triangular and honeycomb lattices. *Phys. Rev. A* **2019**, *99*, 032113. [[CrossRef](#)]
16. Anglés-Castillo, A.; Pérez, A. A quantum walk simulation of extra dimensions with warped geometry. *Sci. Rep.-UK* **2022**, *12*, 1926. [[CrossRef](#)]
17. Kempe, J. Quantum random walks: An introductory overview. *Contemp. Phys.* **2003**, *44*, 307–327. [[CrossRef](#)]
18. Ambainis, A.; Kempe, J.; Rivosh, A. *Coins Make Quantum Walks Faster*; SODA ’05; Society for Industrial and Applied Mathematics: Philadelphia, PA, USA, 2005; pp. 1099–1108.
19. Childs, A.M.; Goldstone, J. Spatial search by quantum walk. *Phys. Rev. A* **2004**, *70*, 022314. [[CrossRef](#)]

20. Grover, L.K. A fast quantum mechanical algorithm for database search. In Proceedings of the ACM symposium on Theory of Computing—STOC '96, Philadelphia, PA, USA, 22–24 May 1996.
21. Lavor, C.; Manssur, L.R.U.; Portugal, R. Grover's Algorithm: Quantum Database Search. *arXiv* **2003**, arXiv:quant-ph/0301079.
22. Abal, G.; Donangelo, R.; Marquezino, F.L.; Portugal, R. Spatial search on a honeycomb network. *Math. Struct. Comp. Sci.* **2010**, *20*, 999–1009. [[CrossRef](#)]
23. Inui, N.; Konishi, Y.; Konno, N. Localization of two-dimensional quantum walks. *Phys. Rev. A* **2004**, *69*, 052323. [[CrossRef](#)]
24. Konno, N.; Obata, N.; Segawa, E. Localization of the Grover Walks on Spidernets and Free Meixner Laws. *Commun. Math. Phys.* **2013**, *322*, 667–695. [[CrossRef](#)]
25. Bezerra, G.A.; Lugão, P.H.G.; Portugal, R. Quantum-walk-based search algorithms with multiple marked vertices. *Phys. Rev. A* **2021**, *103*, 062202. [[CrossRef](#)]
26. Tulse, A. Faster quantum-walk algorithm for the two-dimensional spatial search. *Phys. Rev. A* **2008**, *78*, 012310. [[CrossRef](#)]
27. Brassard, G.; Høyer, P.; Mosca, M.; Tapp, A. Quantum amplitude amplification and estimation. *arXiv* **2002**, arXiv:quant-ph/0005055.
28. Roget, M.; Guillet, S.; Arrighi, P.; Di Molfetta, G. Grover Search as a Naturally Occurring Phenomenon. *Phys. Rev. Lett.* **2020**, *124*, 180501. [[CrossRef](#)]
29. Zylberman, J.; Debbasch, F. Dirac Spatial Search with Electric Fields. *Entropy* **2021**, *23*, 1441. [[CrossRef](#)]
30. Welch, J.; Greenbaum, D.; Mostame, S.; Aspuru-Guzik, A. Efficient quantum circuits for diagonal unitaries without ancillas. *New J. Phys.* **2014**, *16*, 033040. [[CrossRef](#)]
31. Nielsen, M.A.; Chuang, I.; Grover, L.K. Quantum Computation and Quantum Information. *Am. J. Phys.* **2002**, *70*, 558–559. [[CrossRef](#)]
32. Scherer, A.; Valiron, B.; Mau, S.C.; Alexander, S.; van den Berg, E.; Chapuran, T.E. Concrete resource analysis of the quantum linear-system algorithm used to compute the electromagnetic scattering cross section of a 2D target. *Quantum Inf. Process.* **2017**, *16*, 60. [[CrossRef](#)]
33. Portugal, R. *Quantum Walks and Search Algorithms*; Springer International Publishing: New York, NY, USA, 2018.
34. Preskill, J. Quantum Computing in the NISQ era and beyond. *Quantum* **2018**, *2*, 79. [[CrossRef](#)]
35. Zhang, K.; Rao, P.; Yu, K.; Lim, H.; Korepin, V. Implementation of efficient quantum search algorithms on NISQ computers. *Quantum Inf. Process.* **2021**, *20*, 233. [[CrossRef](#)]
36. Douglas, B.L.; Wang, J.B. Efficient quantum circuit implementation of quantum walks. *Phys. Rev. A* **2009**, *79*, 052335. [[CrossRef](#)]
37. Loke, T.; Wang, J.B. Efficient quantum circuits for continuous-time quantum walks on composite graphs. *J. Phys. A-Math. Theor.* **2017**, *50*, 055303. [[CrossRef](#)]
38. Arnault, P.; Debbasch, F. Quantum walks and discrete gauge theories. *Phys. Rev. A* **2016**, *93*, 052301. [[CrossRef](#)]
39. Shikano, Y. From Discrete Time Quantum Walk to Continuous Time Quantum Walk in Limit Distribution. *J. Comput. Nanos.* **2013**, *10*, 1558–1570. [[CrossRef](#)]
40. Arrighi, P.; Nesme, V.; Forets, M. The Dirac equation as a quantum walk: higher dimensions, observational convergence. *J. Phys. A-Math. Gen.* **2014**, *47*, 465302. [[CrossRef](#)]
41. Shakeel, A. Efficient and scalable quantum walk algorithms via the quantum Fourier transform. *Quantum Inf. Process.* **2020**, *19*, 323. [[CrossRef](#)]
42. Devitt, S.J.; Munro, W.J.; Nemoto, K. Quantum error correction for beginners. *Rep. Prog. Phys.* **2013**, *76*, 076001. [[CrossRef](#)]
43. Harper, R.; Flammia, S.T. Fault-Tolerant Logical Gates in the IBM Quantum Experience. *Phys. Rev. Lett.* **2019**, *122*, 080504. [[CrossRef](#)]
44. Roffe, J. Quantum error correction: an introductory guide. *Contemp. Phys.* **2019**, *60*, 226–245. [[CrossRef](#)]
45. Chandrashekar, C.M.; Srikanth, R.; Banerjee, S. Symmetries and noise in quantum walk. *Phys. Rev. A* **2007**, *76*, 022316. [[CrossRef](#)]
46. Banerjee, S.; Srikanth, R.; Chandrashekar, C.M.; Rungta, P. Symmetry-noise interplay in a quantum walk on an n-cycle. *Phys. Rev. A* **2008**, *78*, 052316. [[CrossRef](#)]
47. Alberti, A.; Alt, W.; Werner, R.; Meschede, D. Decoherence models for discrete-time quantum walks and their application to neutral atom experiments. *New J. Phys.* **2014**, *16*, 123052. [[CrossRef](#)]
48. Oliveira, A.C.; Portugal, R.; Donangelo, R. Decoherence in two-dimensional quantum walks. *Phys. Rev. A* **2006**, *74*, 012312. [[CrossRef](#)]
49. Di Molfetta, G.; Debbasch, F. Discrete-time quantum walks in random artificial gauge fields. *Quantum Stud. Math. Found.* **2016**, *3*, 293–311. [[CrossRef](#)]
50. Morley, J.G.; Chancellor, N.; Bose, S.; Kendon, V. Quantum search with hybrid adiabatic quantum-walk algorithms and realistic noise. *Phys. Rev. A* **2019**, *99*, 022339. [[CrossRef](#)]
51. Peng, Y.F.; Wang, W.; Yi, X.X. Discrete-time quantum walk with time-correlated noise. *Phys. Rev. A* **2021**, *103*, 032205. [[CrossRef](#)]